Seismic Inversion Applied to the Evaporites of Bacalhau field, Santos Basin

Gustavo Souza[1], Wagner Moreira Lupinacci[1,2], [1]GIECAR-UFF, [2]INCT-GP

Abstract

The presence of exotic salts in the Santos Basin can have significant technical implications for well drilling and metallurgy. Therefore, it is crucial to accurately identify these salts and determine their thicknesses. This expanded abstract is based on a bachelor thesis involving an acoustic seismic inversion process in the saline section of the Bacalhau Field, Santos Basin. Acoustic impedance can be used to classify salts, estimate thickness, and analyze evaporite mineralogy due to its distinct and contrasting acoustic responses. The workflow involved preconditioning to predict missing density well logs, which are useful for background modeling. An automatic facies classification using the K-means algorithm was conducted to discuss the relationship between saline facies and acoustic response, revealing a strong correlation between acoustic impedance and the three salt groups studied: low-velocity salts (tachyhydrite, carnallite, and sylvite), halite, and anhydrite. The results obtained through seismic inversion in this study provided a detailed geospatial distribution of acoustic impedance, enabling the construction of a 3D model of the evaporites in the Bacalhau Field region. Furthermore, by completing the inversion flow using full azimuth seismic acquisition data, additional inversions were performed using different azimuthal products to discuss isotropy. These inversions revealed similar structures and facies but with variations in thickness.

Introduction

The Bacalhau Field in the Santos Basin is located 185 kilometers offshore at a water depth of 2050 meters. It is operated by Equinor in partnership with ExxonMobil, Petrogal, and PPSA.

The presence of exotic salts in the evaporite section above the pre-salt carbonate reservoirs has significant technical implications for drilling and metallurgy. Salts like tachyhydrite, carnallite, sylvite, and anhydrite have distinct hardness and mobility characteristics that differ from halite and can cause drilling issues such as premature bit wear, wellbore collapse, drill string entrapment, or casing deformation. Predicting the existence and thickness of these salts is crucial to properly planing the wells and avoid project delays and losses.

Teixeira and Lupinacci (2019) demonstrated that in the salts of the Santos Basin, acoustic impedance is directly related to compressional and shear velocities, density, Young's modulus, and Poisson's ratio, and that these properties can be predicted through empirical equations. Therefore, in the case of evaporites, it is possible to save resources by performing an acoustic inversion instead of an elastic inversion.

A seismic survey using ocean-bottom nodes (OBN) was conducted in the Bacalhau Field by CGG in 2020. This OBN provides coverage for all azimuthal angles and long offsets (8 to 37 kilometers). Santos et al. (2022) described that the processing flow for the Full Track Post Stack volume with P-wave and down-going wavefield includes Surface-Related Multiple Elimination (SRME), Internal Multiple Attenuation (IMA), Time-Lag Full Wave Inversion (TL-FWI), anisotropic tomography, and Least Squares Reverse Time Migration (LSRTM). In addition to a full azimuth seismic volume, a series of narrow-azimuth volumes were also provided.

The aim of this work was to perform an acoustic seismic inversion in the saline section of Bacalhau. Acoustic impedance is commonly used for salt classification, thickness estimation, and mineralogy analysis due to the distinct and contrasting acoustic responses of salts. Different narrow-azimuth products were used to examine how different seismic source-receiver pairs affect the inversion and its interpretation compared to the full azimuth inversion.

Bayesian Acoustic Seismic Inversion

The forward modeling of the acoustic seismic case is based on the Aki and Richards (1980) equation, which provides a linear approximation of the reflection coefficients, valid for incidence angles up to 30 degrees. Since the acoustic scenario is a simplification that does not consider elasticity, an incidence angle of 0 degrees is assumed. Thus, the equation depends exclusively on the contrasts of acoustic impedance. The convolution of a wavelet with the reflection coefficients generates a synthetic seismic trace, which reproduces the propagation of a plane wavefront in an acoustic and anisotropic medium with reflective interfaces. Forward modeling is performed by inserting the Aki and Richards coefficients and the wavelet through convolution into a forward modeling operator called G, so that:

$$d_{syn} = G \cdot m \Leftrightarrow m = G^{*} \cdot d_{obs} \quad (1)$$

where m is the parameter matrix, i.e., the acoustic impedances, d_{syn} is the synthetic data, and d_{obs} is the observed data, i.e., the seismic survey data, and G^{*} is the pseudo-inverse of the modeling operator. Acoustic seismic inversion is the inverse process of forward modeling and aims to obtain, from the observed data, the model of parameters.

The solution proposed by Buland and Omre (2003) assumes that the error in the observed data follows a normal Gaussian distribution and is independent of the prior model. The posterior distribution $N(u_{m|post}, C_{m|d_{obs}})$ is given by:

$$u_{m|post} = u_{m_{prior}} + (GC'm|prior)^T C^{-1} d_{obs}(d_{obs} - d_{syn}) \quad (2)$$

$$C_{m|d_{obs}} = C'm + (GC'm|prior)^T C^{-1} d_{obs} GC'_m \quad (3)$$

where $u_{m|prior}$ is the prior model containing the low-frequency geological information. G is the modeling matrix, d_{obs} is the observed amplitude, and d_{syn} is the synthetic amplitude calculated from the prior model. The difference between d_{obs} and d_{syn} represents the residual. C_*^n are the covariance matrices of n order that derivatives of m, d_{obs}, or d_{syn}. The posterior distribution, derived explicitly, provides the complete solution to the inverse problem, including uncertainty. The solution employed is the Maximum A Posteriori (MAP) estimate, represented by:

$$MAP[\exp[m]] = \exp[u_{m|d_{obs}} - \sigma^2_{m|d_{obs}}], \quad (4)$$

where $\sigma^2_{m|d_{obs}}$ is the posterior variance. Typically, $\sigma^2_{m|d_{obs}}$ is greater than $u_{m|d_{obs}}$, ensuring that the log-Gaussian distribution is approximately symmetric, and $\exp[u_{m|d_{obs}}]$ is a good approximation for $MAP\exp[m]$.

Methodology

The methodology employed involved a preconditioning step of compressional velocity and density profiles, both used to obtain acoustic impedance. Next, a facies classification using K-means was conducted to evaluate if these profiles could identify different types of salts. This was followed by well ties since seismic inversion occurs in the time domain while well data are originally in depth. Subsequently, a low-frequency model, used as an a priori model, was constructed using a low-pass filter and geostatistics. Finally, the inversion was performed for the full-stack and full-azimuth volumes and then with the azimuthal products.

Well logs preconditioning

Despike filters were applied to remove spurious values, and sections with missing density data were filled prediction. Density profiles are usually predicted using regression with compressional sonic through a empirical equation by Gardner et al. (1974), but this equation is sensitive to lithology type. Moreover, using only one independent variable introduces common regression implications. Therefore, a machine learning approach based on decision trees was used. This approach allows the use of additional logs besides the sonic, such as gamma-ray logs. These additional logs mitigate the sensitivity of density to lithology types. Different ML models were tested, and XGBoost performed the best with a correlation of 0.82 compared to 0.70 for linear regression.

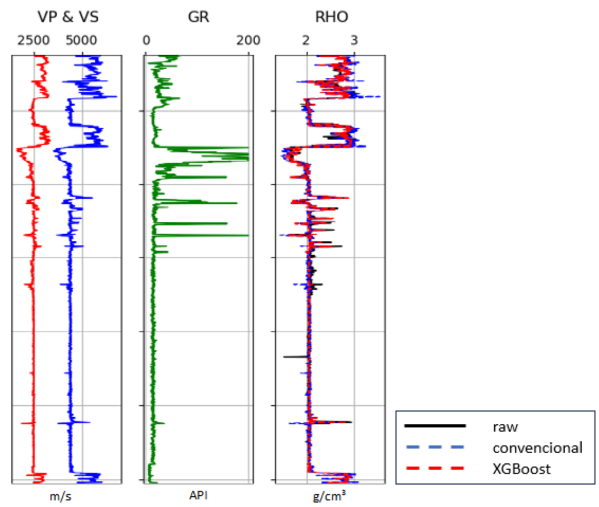

Figure 1: Well log panel. First track: with P-velocity in blue and S-velocity in red. Second track: gamma ray in green. Third track: Raw density in black, predicted density with convencional aproach in blue and predicted density with XGBoost in red.

Well tie

In this project, statistical wavelets were extracted with a sample count of 65 and a 5-sample interval within a 50-meter region around each well, corresponding to the seismic time interval of the salt. These wavelets were tested, and it was observed that using a Ricker wavelet with the same dominant frequency as the statistical wavelet increased the correlation coefficient. The wavelet frequencies varied from 19Hz to 23Hz.

Table 1: Correlation Coefficients

Well Name	Wavelet	Frequency	Correlation
Well A	Ricker	23 Hz	52,8%
Well B	Ricker	21 Hz	54,2%
Well C	Ricker	19 Hz	60,6%

Background model

The a priori model was constructed considering three guiding horizons: the top of the salt, intra-salt, and the top of the anhydrite. The top of the anhydrite was interpreted instead of the actual base of the salt (top of the reservoir) because the tuning effect blends that reflections. The intra-salt horizon was interpreted because salt layers do not follow only the top and base; additionally, in salt domes, the layers have particular inclinations. A shift of 200 meters above the base of the salt and 200 meters below the anhydrite applied, this shift is larger than the wavelet size, allowing the reflections in the salt interface to appear in the convolutional model used in the inversion process. Wells A and B were inserted in the background model and well C served as a blind well.

Inversion parameters

The algorithm by Buland and Omre (2003) uses signal-

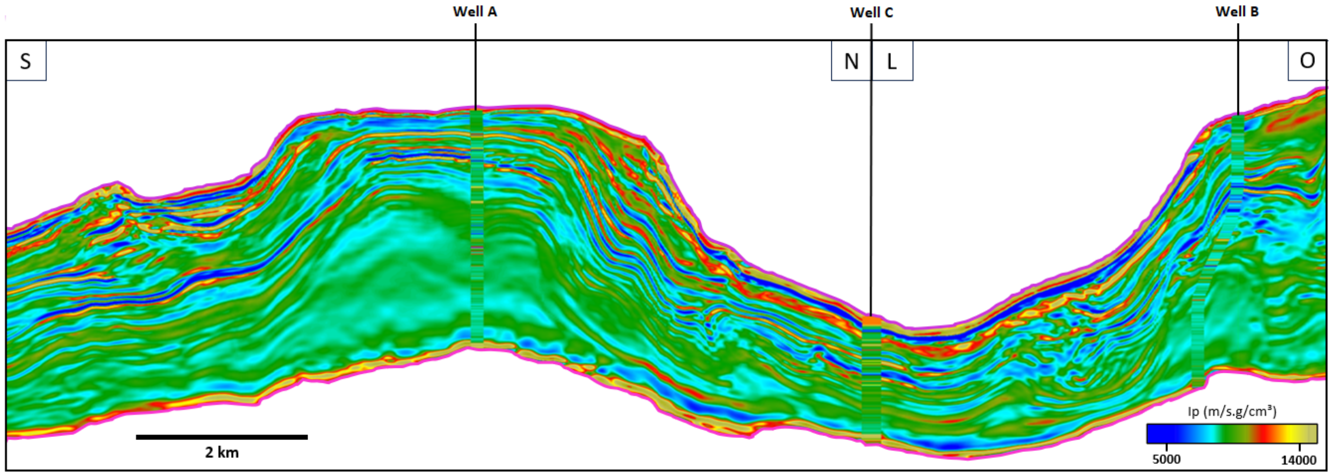

Figure 2: Section of acoustic impedance generated with full-stack full-azimuth volume crossing 3 wells with unscaled wells. Wells A and C are control wells, well B is a blind well.

to-noise ratio and a scalar for wavelet parameterization as input parameters. These are the primary variables for modifying the inversion. Values of $S/N = 60$ and $Scale = 40000$ were selected iteratively, using the inversion results at the control wells as indicators. Covariance matrices were calculated using data from the two control wells. The wavelet used was a 21Hz Ricker wavelet, chosen for being an intermediate frequency of the wavelets used in the tying of the three wells. The seismic inversion generated five acoustic impedance cubes: one for the full azimuth and four for each azimuthal section.

Results and Discussion

The results in this work were analyzed using a single arbitrary line that crosses the three wells in the southern portion of Bacalhau. The seismic inversion result compared with the logs of the control wells showed maximum acoustic impedance correlation at the basal anhydrite of the two control wells. The region with low reflection occurrence just above the basal anhydrite was dominated by the trend imposed by the low-frequency model, without direct correlations between well and the inversion cube. A thick layer of low acoustic impedance salts, confirmed by the composite profile as carnallite, is revealed with its lateral continuity and thickness around the two control wells region. In control well A, there is a thin layer with higher acoustic impedance than halite, an indication of anhydrite confirmed by the composite profile. However, the values are not on the same scale as the basal anhydrite and top anhydrite, which are considered purer. The acoustic impedance around $12000 g/cm^3 \cdot m/s$ indicates that the composition is not entirely pure, likely containing a percentage of halite. The occurrence of this acoustic impedance anomaly is even lighter in well C, indicating a lateral decrease in the presence of this salt from portion A to C. The top anhydrites of the two control wells have high acoustic impedance values and on the same scale, both in the wells and in the obtained volume.

The blind well does not have the low reflection region as in the control wells, so its entire saline interval can be evaluated. Starting from the base, the anhydrite is aligned, both in thickness and in acoustic impedance value, approximately $18000 g/cm^3 \cdot m/s$. The impedance values just above represent halite with minor variations, indicating a mixed composition with low salts. Just above halite, there are some contrasts between low salts and anhydrite, with lateral continuity in the impedance cube and directly correlated with the blind well. At the top, which has a sequence of 3 considerably thick layers of anhydrite, low salt, and top anhydrite respectively. The anhydrite prior to the low salt represented in well profiles as intercalations between anhydrite and halite. The blind well demonstrated that the inversion successfully revealed the spatial characteristics of acoustic impedance, enabling a 3D interpretation of the evaporites in this region.

The seismic inversion succeeded in recovering the acoustic impedances on scales compatible with those found in well profiles. The acoustic impedance volume (Figure 2) reveals the geospatial distribution of impedance, allowing interpretation of the lateral continuity of the different salts. To identify which impedance values are associated with each salt, Figure 4.A demonstrates a facies classification via K-means. The K-means algorithm is an unsupervised clustering method widely used in various areas for data analysis, machine learning, and pattern recognition MacQueen (1967). It separated the dataset into 3 groups: low impedance salts, halite, and anhydrite. Each group is represented by a centroid, which is a point in the data space that represents the average center of the points in the group. This separation is possible because the composite profile indicated a sharp separation between facies based on Vp, Vs, and RHO profiles.

The distribution of impedance for the 3 facies indicates that halite has a mean acoustic impedance value around $9218 g/cm^3 \cdot m/s$, with a standard deviation of $5667 g/cm^3 \cdot m/s$. Low acoustic impedance salts have a standard deviation of $973 g/cm^3 \cdot m/s$ and anhydrite $1629 g/cm^3 \cdot m/s$. The separation between halite and anhydrite has a strong contrast, where we can assume that values above $11000 g/cm^3 \cdot m/s$ have almost no probability of being halite. On the other hand, salts below $8000 g/cm^3 \cdot m/s$ can be classified as low acoustic impedance salts. Additionally, Figure 4.B demonstrates that Ip and Is have

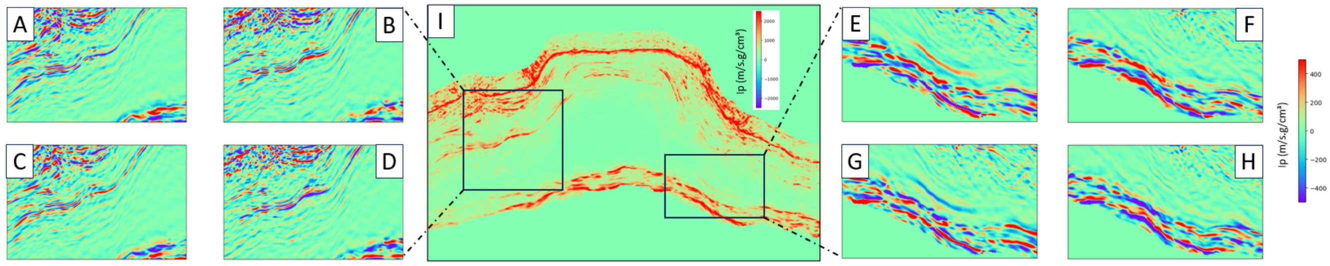

Figure 3: I) Section with the accumulated sum of the absolute differences of each acoustic impedance volume from the four azimuthal sections in relation to the acoustic impedance volume generated by full azimuth. Rectangles A/E, B/F, C/G, and D/H are the relative differences between sections 01, 02, 03, and 04, respectively, and the full azimuth.

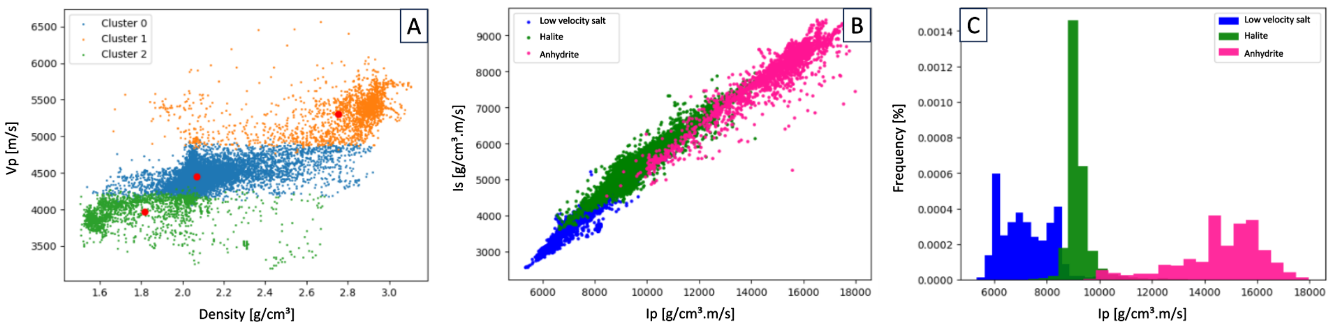

Figure 4: Facies grouped by K_{means}. A) Crossplot of Vp vs density, colored by cluster. Centroids in red. B) Crossplot of impedance of S-wave vs impedance of P-wave colored by facies. C) Acoustic impedance histogram of the saline facies

an approximately linear relationship, demonstrating that there is no need to use shear information to distinguish the different types of salts.

Based on well information, the blue color in the inversion is associated with low acoustic impedance, indicating salts such as tachyhydrite, carnallite, and sylvite, while red and yellow colors are associated with anhydrites with high acoustic impedance. As a background, the green color indicates halite, the most abundant salt in the evaporitic section of the Santos Basin. The arbitrary section in Figure 2 illustrates that low salts are present in considerably thick layers throughout the field's extent.

All azimuthal impedance cubes were extracted with the same parameters as the full-azimuth volume inversion. The acoustic impedances of the azimuthal cubes share the same saline structure as the cube generated by full azimuth. As observed in Figure 3, the differences between impedances are less expressive for the larger extent of the volume and only have truly significant values in low acoustic impedance salts and with differences that follow the lateral extent of these facies. These differences vary between -500 and 500 $m/s \cdot g/cm^3$.

Based on Figure 3, the largest quantitative discrepancies are observed in low velocity salts south of the arbitrary line and in the anhydrite of the northern flank relative to the position of control well A. In the first case, azimuthal section 02 indicates a greater thickness of carnallite, while section 04 indicates the opposite. In the case of differences observed in the flank, section 01 highlights a greater thickness of anhydrite, while section 03 underestimates this thickness. However, in the same flank, closer to the base, a layer of high acoustic impedance present in the full azimuth has lower values compared to section 01 and a positive difference compared to section 03. This demonstrates that depending on the azimuth, it can both underestimate and overestimate the acoustic impedance compared to the full stack result.

Conclusions

Based on the results of the seismic inversion, it was possible to obtain the geospatial distribution of acoustic impedance, resulting in the 3D compression of evaporites in the Bacalhau Field. The facies classification in the wells demonstrated a strong relationship between acoustic impedance and the three groups of salts studied: low-velocity salts (such as tachyhydrite, carnallite, and sylvite), halite, and anhydrite.

The step of predicting missing profiles, such as velocities and density, was crucial for the completion of the seismic inversion workflow. Accurate prediction of these profiles is essential since they are used in constructing the low-frequency model, directly influencing the final result. Compared to the conventional regression approach, predictive models using decision tree family methods achieved better performance indicators.

Moreover, the seismic inversion workflow with the different azimuthal products showed that the azimuthal sections reveal the same structures and salt facies as the full azimuth, but with different thicknesses and acoustic impedance values. The acoustic impedances ranged between -500 and 500 m/s.g/cm³, which may affect the interpretation between cleaner halite and halite with mixed salts. These differences may be associated with the isotropy.

The results of this work exemplify the potential of seismic inversion in contributing to the understanding of local geology and in planning new wells in the region. Besides transforming an interface property into layers, seismic inversion provides useful information on thickness, composition, and facies. This information is important for the engineering team to understand the physical stresses against the well structures, ensuring safer drilling operations and reducing risks in well design. Additionally, from this work, new petrophysical parameters could be calculated from the tree dimensional impedance inverted model.

Acknowledgments

I am grateful to Equinor for providing the necessary data and resources for this project and to GIECAR for their guidance and machine learning algorithms.

References

Aki, K., and P. G. Richards, 1980, Quantitative seismology: [S.l.: s.n.].

Buland, A., and H. Omre, 2003, Bayesian linearized AVO inversion: GEOPHYSICS, **68**, 185–198.

Gardner, G., L. W. Gardner, and A. R. Gregory, 1974, Formation velocity and density - The diagnostic basis for stratigraphic traps: Geophysics, **39**, 770–780.

MacQueen, J. B., 1967, Some methods for classification and analysis of multivariate observations: Proc. of the fifth Berkeley Symposium on Mathematical Statistics and Probability, University of California Press, 281–297.

Santos, P., E. Schwedersky, C. Hess, K. Sundøy, and C. Franca, 2022, Bacalhau OBN: Equinor's first deep-water node seismic: Presented at the Third EAGE Conference on Pre Salt Reservoirs, European Association of Geoscientists & Engineers.

Teixeira, L., and W. M. Lupinacci, 2019, Elastic properties of rock salt in the santos basin: Relations and spatial predictions: Journal of Petroleum Science and Engineering, **180**, 215–230.